Passive scalar mixing studies to identify the mixing length in a supersonic confined jet

Article *in* Experiments in Fluids · April 2017

DOI: 10.1007/s00348-017-2342-x

4 authors:

Sengunthapuram Kandasamy Karthick
Technion - Israel Institute of Technology
57 PUBLICATIONS **221** CITATIONS
SEE PROFILE

Srisha M.V. Rao
Indian Institute of Science
76 PUBLICATIONS **448** CITATIONS
SEE PROFILE

Jagadeesh Gopalan
Indian Institute of Science
297 PUBLICATIONS **2,376** CITATIONS
SEE PROFILE

K P J Reddy
Indian Institute of Science
268 PUBLICATIONS **1,996** CITATIONS
SEE PROFILE

RESEARCH ARTICLE

Passive scalar mixing studies to identify the mixing length in a supersonic confined jet

S. K. Karthick • Srisha M. V. Rao • G. Jagadeesh • K. P. J. Reddy

Received: 2 February 2017 / Revised: 22 March 2017 / Accepted: 4 April 2017

Abstract Supersonic jet with a co-flow, closely bounded by walls is known as supersonic confined jet. Supersonic confined jet is encountered in practical devices like the supersonic ejector. Mixing of the primary and the secondary fluid inside the confined passage is complex. From a design perspective, it is necessary to have an accurate knowledge of the mixing length (L_{MIX}). Tracers that do not actively participate in the flow behavior but rather mark the fluids such that they faithfully follow the fluid motion are known as passive scalars. Passive scalars help in the understanding the progression of mixing amidst interacting flows. In this work, we have performed passive scalar mixing studies in a supersonic confined jet for different operating conditions using an existing low area ratio (AR=3.7) rectangular supersonic gaseous ejector. Air is used as the working fluid in both the primary and the secondary flow. The design Mach number of the primary flow nozzle (M_{PD}=1.5–3.0) and the total pressure of the primary flow (P_{OP}=4.89–9.89 bar) are varied during the experiments. Using the planar laser-induced fluorescence (PLIF) technique and acetone as the passive scalar, L_{MIX} is determined. A 266 nm Nd-YAG laser with a repetition rate of 8 Hz is used to excite the acetone molecules in the flow field, and the emitted fluorescence is captured by an ICCD camera. A new method is proposed to study the passive scalar distribution from the acetone PLIF images through digital image processing. Spatial Scalar Fluctuations Intensity (SSFI or ψ) is a parameter defined at every transverse section along the flow direction. Based on the variation of ψ along the jet, the location of L_{MIX} can be identified. L_{MIX} is defined as the length from the supersonic nozzle exit where ψ first attains a value of 0.05. For the first time, L_{MIX} is quantified in a supersonic confined jet. L_{MIX} values are observed to be in the range of 3H to 6H for the cases under study, where H is the height of the confined passage. The behavior of L_{MIX} is closely dependent on the nozzle operating conditions. The values of L_{MIX} are found to be reduced by 17.67% for the over-expanded flows and increased by 15.76% for the under-expanded flows from the perfectly expanded condition. This study also provides other supersonic confined jet characteristics like the potential core length (L_{PC}) and the shock cell spacing (S_x) of the primary supersonic jet. Compared to the supersonic free jet, values of L_{PC} and S_x are found to be different in the supersonic confined jet.

1 Introduction

Gaseous mixing at supersonic speeds is critical in the development of supersonic combustion chambers (Vishwakarma and Vaidyanathan 2016) for air-breathing engines and supersonic gaseous ejectors (Rao and Jagadeesh 2015) for rapid fluid mixing. The fact that mixing at supersonic velocities is considerably reduced (Papamoschou and Roshko 1988; Clemens and Mungal 1995) in comparison to low speed is well known, but the underlying gasdynamic phenomena responsible for supersonic gaseous mixing is not well understood. Targeted studies on supersonic gaseous mixing are carried out on compressible free jets (Rao et al. 2016), transverse jets (Desikan et al. 2015), impinging jets (Brehm et al. 2016) and confined jets (Karthick et al. 2016a). In particular, we are concerned with supersonic confined jet where a primary supersonic jet with a co-flowing secondary stream is closely bounded by walls. Complexities of growing mixing layers and boundary layers, shock interactions with the mixing layer, and the development of secondary flow inside the bounded passage, make the studies in supersonic confined jet significantly difficult in comparison with other canonical mixing flow problems (Slessor et al. 2000). Added to that, the compressible mixing process is three-dimensional and unsteady.

Gasdynamics of gaseous mixing within a typical supersonic confined jet configuration is the focus of current study. Supersonic confined jets are used in many applications, including propulsive devices (Heiser 2010), wind tunnel testing facilities (Kracik et al. 2014), high altitude testing facilities (Sankaran et al. 2000) (HAT), gas-dynamic lasers

✉ S. K. Karthick (ORCID ID: 0000-0003-1285-9771)
skkarthick@ymail.com

Department of Aerospace Engineering, Indian Institute of Science, Bangalore – 560012, India

(Singhal et al. 2010), and fuel cells (Rao and Jagadeesh 2010) in the form of ejectors. Few recent attempts (Rao and Jagadeesh 2014; Karthick et al. 2015b; Karthick et al. 2015a; Karthick et al. 2016a) have been made to study the supersonic mixing layers observed in supersonic confined jet like configurations. Supersonic confined jets encountered in practical applications have a low Area Ratio (AR<5) (Mazzelli and Milazzo 2015) which is defined as the ratio of the sectional mixing duct area and the primary nozzle exit area. Nature and flow dynamics associated with the development of mixing layer in a low AR supersonic confined jet is not studied from the standpoint of fluid mixing. The prominent reason could be the blockage offered by the conventional probing technique to investigate such flow field. In recent days, experiments have been carried out with modifications to the conventional intrusive measurement techniques (Desevaux et al. 1994). However, they continue to compromise the flow field to a smaller extent. Wall mounted static pressure measurements (Chong et al. 2014; Rao and Jagadeesh 2014; Karthick et al. 2016a) shed information on the overall thermodynamic performance of the confined jet, and to some degree on the fluid mixing.

Optical diagnostic tools are non-intrusive methods to study such complex flows. Conventional optical diagnostics like Schlieren visualization (Rao and Jagadeesh 2014; Chen et al. 2015) poses limitations, as the acquired image is line-of-sight integrated. It is hard to infer details of fluid mixing from such flow visualization technique, as it solely relies on the derivatives of density in the flow field. Nonetheless, in the recent work of Rao and Jagadeesh (2014), extensive digital image processing on Schlieren images enabled the computation of non-mixed length (L_{NM}) in the supersonic confined jet. They define the L_{NM}, as the length up to which the primary and the secondary flow are distinctly identifiable using the definition of a mixing parameter – β_{mix}. They have also validated the observations of L_{NM} from the Schlieren experiments through the Planar Laser Mie Scattering (PLMS) experiments (Tropea et al. 2007). Later, using a similar approach, the authors (Karthick et al. 2016a) have performed a parametric study on a supersonic confined jet, and they have provided the changing trend of L_{NM} for a broad range of operating conditions by seeding the primary flow alone. Using similar analogy for the estimation of L_{NM}, the authors have also computed the potential core length (L_{PC}) of the primary supersonic jet, by seeding the secondary flow alone to understand about the non-mixed region in the supersonic confined jet. However, these previous works yielded only the location of the L_{NM} inside the supersonic confined jet. While this information goes a long way in addressing the key design questions of what is the length of the mixing duct in a supersonic confined jet, it does not solve the problem completely. Partly, this is because Mie scattering does not distinguish between particles being seeded and particles otherwise present in the flow. Even though particles are seeded in the primary flow alone, condensing particles in the secondary flow can interfere with the interpretation of flow images. Even in some cases, due to rapid nucleation (Ding et al. 2014a; Karthick et al. 2016a), the flow is self-seeded, and it limits the calculation of L_{PC} for a broad range of operating conditions. Therefore, the length of the complete mixing of two fluids in a supersonic confined jet is still an open question.

Passive scalar studies are preferred to study the turbulent mixing field (Warhaft 2000). On looking at the literature for other choices of non-intrusive scalar measurement techniques that are carried out especially in supersonic flows through wall bounded passage (Plesniak and Cusano 2005), like the case under study, acetone Planar Laser Induced Fluorescence (PLIF) (Vancruyningen et al. 1990; Lozano et al. 1992; Thurber et al. 1998; Thurber and Hanson 1999; Rao et al. 2016; Stetsyuk et al. 2016) is found to be an appropriate candidate. The flow field is seeded with a suitable tracer. The tracer emits fluorescence upon excitation by a laser light sheet of a particular wavelength. The emitted fluorescence intensity is directly proportional to the local number density of the tracer (Houwing et al. 1996; Thurber and Hanson 2001; Handa et al. 2011) in the flow field, thereby marking the local concentration of the tracer under study. Thus, this method eliminates the ambiguity arising from the nucleating or condensing particles in the flow stream, and offers better understanding of the mixing process. Acetone PLIF technique has been employed to study supersonic fluid mixing in both reacting hot flows (Sun et al. 2009) and non-reacting cold flows (Takahashi et al. 2008). A 266 nm wavelength laser light is used to excite acetone tracers in the PLIF experiments. In incompressible free jets, acetone PLIF technique is used to identify the local concentration field (Vancruyningen et al. 1990) and the dissipation rate (Lozano et al. 1992). However, absolute quantification of concentration field, especially in terms of mixture fraction, in a compressible shock laden jets is much involved due to the dependency of acetone fluorescence (Thurber and Hanson 1999; Bryant et al. 2000; Thurber and Hanson 2001) with respect to local temperature, pressure and concentration. Along with that, the decrement in fluorescent image intensity with increase in tank or total pressure and due to acetone condensation at low static temperature while investigating a supersonic free jet using acetone PLIF is also shown (Shelar et al. 2014b) to be prominent. Hence, additional care is required to quantify the absolute local concentration of the flow field. Disregarding the acetone fluorescence dependencies in the compressible flow field will introduce substantial errors and uncertainty in the quantitative data analysis.

The current objective of our experiments is to determine the L_{MIX} in a supersonic confined jet. As the fluorescent intensity is proportional to acetone concentration in the flow field, it clearly marks the region of non-mixed or mixed region depending upon the flow seeding either in the primary flow or the secondary flow. The region of complete mixing or L_{MIX} is identified when the fluorescent intensity is observed to be uniform across the duct height (H). Our aim is to quantify the exact location of the above-said occurrence. In this regard, absolute quantification of local concentration is not necessary. A new method is proposed to identify the L_{MIX}

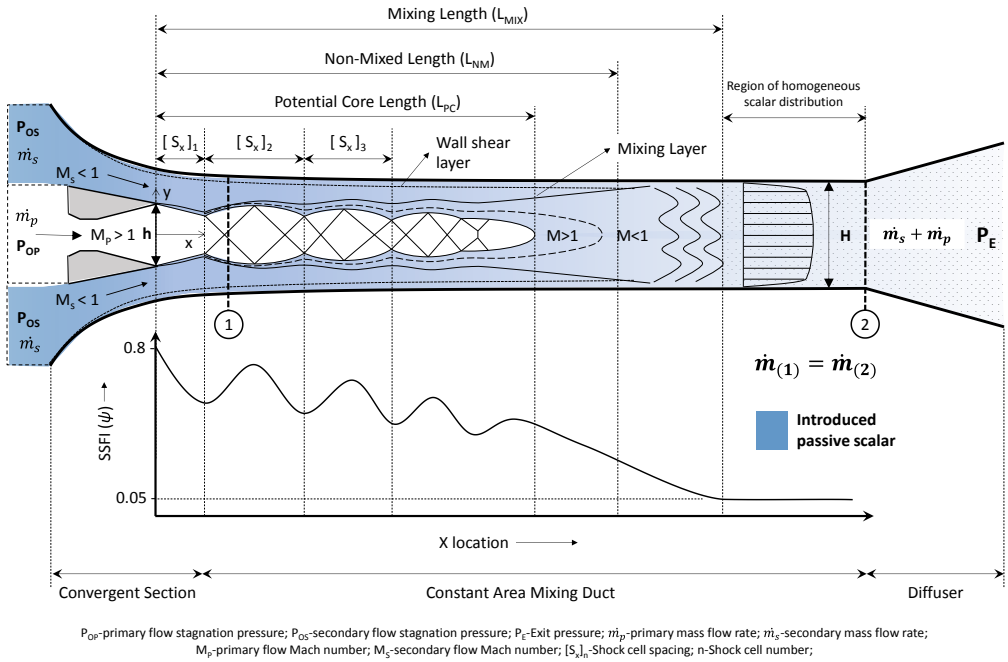

Fig. 1 Schematic of the time-averaged supersonic confined jet depicting basic flow features along with appropriate nomenclature. It has to be noted that mass flow rate in section – 1 and section – 2 remain the same, unlike the free jet

from the acetone PLIF images through digital image processing. Using the definition of Spatial Scalar Fluctuations Intensity (SSFI or ψ) at every transverse sections as a convenient formulation to study the degree of unmixedness (Danckwerts 1952; Spiegler et al. 1976; Dimotakis and Miller 1990; Fric 1993), L_{MIX} is determined in the supersonic confined jet for the first time. The longitudinal location where ψ of 0.05 is first observed marks the L_{MIX}. Through this definition, we can unambiguously determine L_{MIX} from the acetone PLIF images. Schematic of the typical time-averaged flow field seen in the central plane of the supersonic confined jet and the variation of the computed ψ along the jet is clearly illustrated in Fig. 1. The alternate peaks and valleys observed in the variation of ψ demonstrate the location of the successive shock cells in the supersonic primary jet. Several aspects like the driving supersonic primary flow, entrained subsonic secondary flow, the formation of multiple shock cells, growing mixing layer from the tip of the nozzle, developing boundary layer near the wall, and the location of complete mixing between the primary and the secondary flow is marked in Fig. 1. The introduced passive scalar (represented in dark blue color) at the beginning of the secondary flow is shown to be diluted along the primary jet stream (represented in light blue color). It can be seen that the distribution of passive scalar is homogeneous across the duct height at L_{MIX}. Other flow features like the potential core length (L_{PC}) of the primary flow, the non-mixed length (L_{NM}), and the shock cell spacing (Franquet et al. 2015) (S_x) are also clearly shown.

The definition of ψ and the procedure to quantify the L_{MIX} for different operating conditions is one of the major contributions of this paper. The scaling and the non-dimensionalization procedures that are prescribed in Karthick et al. (2016a) will be followed here to represent the entire experimental matrix. Digital image processing routines for acetone PLIF images is briefly described in this article. Acetone PLIF images acquired through the seeding of secondary flow alone offers more insight into characteristics of the supersonic confined jet like L_{PC} and S_x, and its importance is brought out in detail. L_{PC} is determined for a broad range of operating conditions using PLIF and validated with the previous PLMS studies. The behavior of L_{PC} at severely under-expanded flows of the primary nozzle at M_{PD}=1.5 is compared with the free jet. Similar to L_{PC} observations, S_x variations for different nozzle operating conditions encountered at M_{PD}=2.0 is analyzed, and the different trends are compared and contrasted with the supersonic free jet.

Apart from the introduction in Sec. 1, this article contains the broad description of the experimental facility, measurement methodology and operating conditions in Sec. 2. In Sec. 3, steps involved in the data analysis of wall static pressure measurements, acetone PLIF images and the uncertainty encountered in these experiments are given. Major observations and discussions are given in Sec. 4. In the subsection, variations in L_{MIX}, L_{PC} and $[S_x]_n$ for different operating conditions are reported. The last section carries the major conclusions of this paper. Followed by that, a small section is

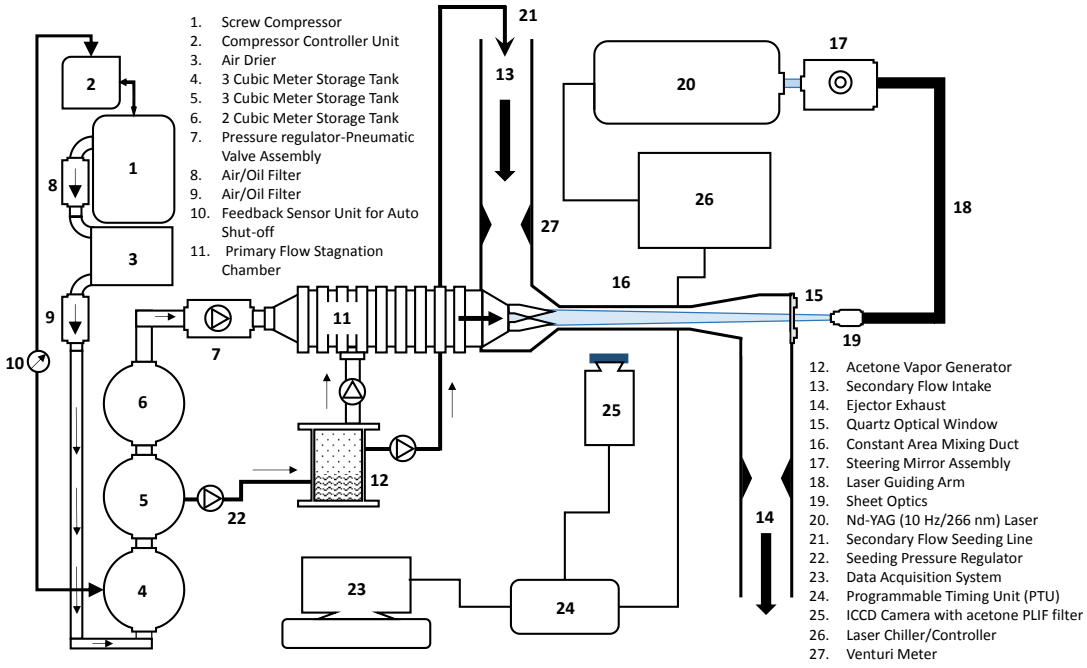

Fig. 2 Schematic illustration of the experimental arrangement for the supersonic confined jet studies using acetone PLIF with associated accessories

given for the nomenclatures used in this article for the convenience of the reader.

2 Experimentation

2.1 Facility

Supersonic confined jet experiments are carried out using the existing supersonic gaseous ejector facility in LHSR, IISc – Bangalore. The supersonic ejector facility has two major components: an Intermittent blow down facility and a supersonic gaseous ejector rig. More details regarding the rigging of the establishment can be seen in the work of Rao (2013); Rao and Jagadeesh (2014). In the following section, a brief introduction regarding the blow-down facility, confined jet configuration, details about pressure measurements, acetone-PLIF arrangements, and operating conditions for the considered experimental matrix will be discussed. Schematic illustration of the experimental arrangement where the supersonic confined jet studies are carried out is given in Fig. 2.

2.1.1 Intermittent Blow-down Facility

The intermittent blowdown facility consists of 22 kW controllable screw compressor to charge the storage tank of 8 m^3 in volume up to 12.5 bar. Before storing the compressed air in the storage tank, the feed line passes through a refrigeration type drier to remove excess moisture content in the compressed air to avoid condensation along the viewing window when the flow expands through the convergent-divergent (CD) nozzle at the supersonic speed. An appropriate set of filters is also used along the feed line for the removal of micron-sized oil and water particles before storing the compressed air in the tanks. Compressed air from the storage tanks is taken into the plenum chamber through a pressure regulator and a pneumatic rotary actuator. The total pressure (P_{OP}) of the primary flow is measured at the end of the plenum chamber. The plenum chamber also has a provision in the initial section for injecting and mixing the tracer particles (acetone vapors) for acetone-PLIF into the primary flow.

2.1.2 Supersonic Confined Jet Module

The supersonic confined jet module is set up at the end of the plenum chamber of the blow-down facility. In general, the supersonic confined jet consists of three parts: a. Converging section b. Constant area mixing duct and c. Diffuser (Fig. 1). For the current experiments, a rectangular supersonic gaseous ejector having a low AR of 3.56 is used (Fig. 2) to study the supersonic confined jet like configuration, where the primary flow coming out of the CD nozzle is at supersonic speed. Area ratio of the supersonic confined jet is defined as given in Eq. 1 (Where, W = width of the confined flow passage; w = width of the primary nozzle flow passage; H = height of the constant area mixing duct; h = exit height of the primary CD nozzle).

$$AR = \left(\frac{W}{w}\right)\left(\frac{H}{h}\right) \quad (1)$$

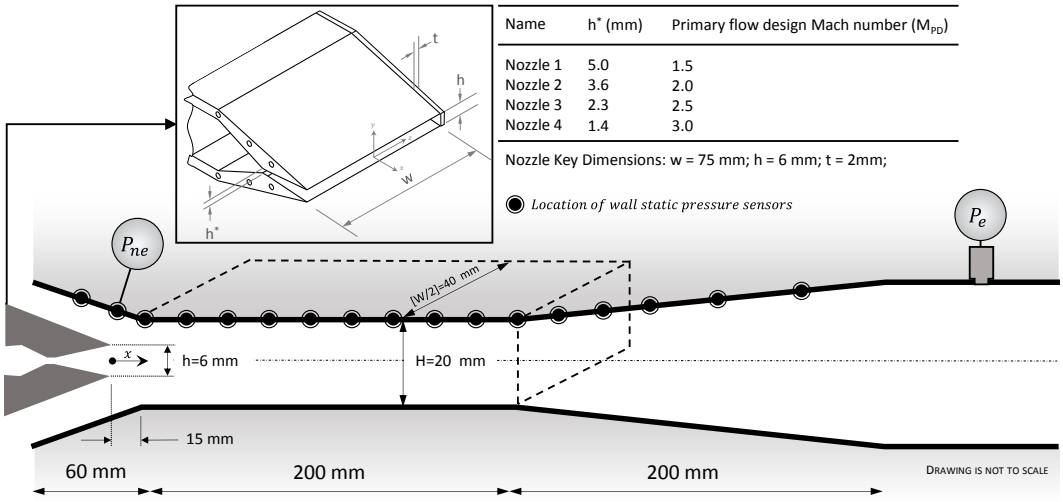

Fig. 3 Critical dimensions of the supersonic confined jet with wall static pressure measurement locations are shown. Sizing parameters of the convergent-divergent (CD) nozzle to accelerate the primary flow to different supersonic design Mach numbers (M_{PD}) are also provided

The nozzle is kept away by 15 mm from the constant area mixing duct. The entrained jet from the ambient conditions enters the confined passage through the convergent section, get mixed with the primary jet in the constant area mixing duct and leaves through the diffuser at the exit. Fig. 1 and Fig. 3 depicts the flow passages encountered in the supersonic confined jet. The nozzle pressure ratio (NPR = P_{OP}/P_{ne}) is monitored by monitoring the pressure (P_{OP}) in the plenum chamber and the pressure around the primary flow nozzle exit (P_{ne}). The values of P_{ne} is obtained by putting a pressure sensor near the nozzle flow exit, on the top wall of the confined passage as shown in Fig. 3 and the major dimensions associated with the supersonic confined jet are also clearly shown there.

2.2 Measurement Methodology

2.2.1 Pressure Measurements

Conventional centerline pressure measurements using Pitot probes in the low area ratio supersonic confined jets are challenging due to spatial constraints or blockage in the probing area. With some novel modifications, a few attempts have been made in the recent days (Desevaux et al. 1994; Ariafar et al. 2014) to measure the centerline static pressure variations. Most of the investigations carried out in the low area ratio supersonic confined jets employ wall static pressure measurements (Dvorak and Safarik 2003; Chunnanond and Aphornratana 2004) to avoid flow intrusion and to extract reasonable details regarding the flow physics. In the current experiments, wall static pressure measurements are carried out particularly to find the location of L_{MIX}. A Piezo-resistive type pressure sensor (MPX5700 ASX) from Freescale™ Semiconductor is used to acquire wall static pressures. These sensors can measure pressure from 15 kPa to 700 kPa (response time of 1 ms with an accuracy of ±2.5%). They are flush mounted one after another along the center plane (z=0) of the supersonic confined jet. Two sensors near the primary flow nozzle region, ten sensors in the constant area mixing duct and five sensors in the diffuser are placed to monitor the wall static pressure variation. The location of pressure sensors for the wall static pressure measurements are shown clearly in Fig. 3. The same pressure sensors are used on the venturi arrangements placed in the entrance and in the exit of the supersonic confined jet module (Fig. 2) to measure the entrained and the mixed mass flow rate. Both the primary and the secondary flow stagnation pressures (P_{OP} & P_{OS}), along with the final exit pressure (P_e) of the mixed flow are monitored using another set of appropriate pressure gauges (IRA-PRA300M). These sensors can measure both gauge and absolute pressure ranging from 10 – 20 bar (response time of 300 ms with an accuracy of ±0.5%). More detail regarding the signal processing, data acquisition and uncertainty are given in the upcoming sections (Sec. 3.1 & Sec. 3.3).

2.2.2 Acetone PLIF

In the area of investigation, one of the mixing flow (either the primary flow or the secondary flow) is seeded with acetone vapors (Thurber and Hanson 2001; Shelar et al. 2013; Shelar et al. 2014a) well before entering the constant area mixing duct. A 266 nm Nd-YAG laser with an energy of 90 mJ per pulse, operating at 8 Hz is used to excite the acetone molecules in the flow-field. The laser beam (<10mm beam width) is focused (f=-50 mm) and collimated using appropriate sheet optics. The collimated laser sheet has a constant height of 25 mm and a thickness of 0.8 mm. The produced laser sheet is then passed through the quartz window present at the exit of the diffuser (Fig. 2). Imaging is done along the flow direction (xy plane) at the center plane (z=0) of the supersonic confined jet. The side walls of the

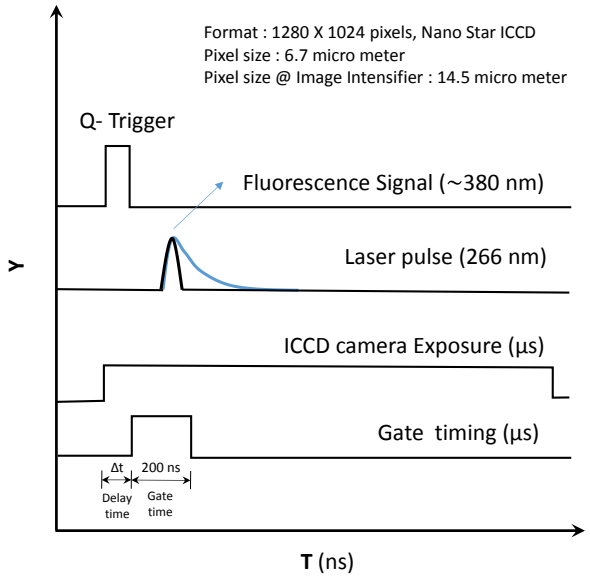

Fig. 4 Typical timing diagram associated with the procedure of acetone PLIF imaging in the investigation of supersonic confined jet using an ICCD camera and the band-pass filter

confined passage are covered with another quartz window for optical access. Gated ICCD (Intensified Charge-Coupled Device) camera with a pixel resolution of 1280 X 1024 pixels (6.7 µm/pixel) captures the fluorescence signal with SNR (Signal to Noise Ratio) greater than 200, at the maximum frame rate of 8 Hz. An acetone PLIF band pass filter with 90% optical transmission at 350 nm, is used to collect the emitted fluorescence signal from the acetone molecules alone. PTU (Programmable Timing Unit) connected to a computer, syncs the laser pulse and the ICCD camera. A gate time of 200 ns is used with appropriate delay to capture the PLIF signals better. Delay timing and gate timing are sensitive in the acetone PLIF procedures. Extreme care has to be taken while performing this operation. A detail timing diagram associated with acetone PLIF imaging procedure is shown in Fig. 4. Acquired acetone PLIF images are pre and post processed in DaVis 8.3 for quantifying L_{MIX} after the spatial calibration of the flow-field. Typical run-time achieved during the testing is around 3 s which is calculated based on the steady conditions of the supplied P_{OP} in the supersonic confined jet. Nearly 50 instantaneous images are captured during the successive runs which are found to be statistically converging to represent the mean scalar flow-field (time-averaged image). A typical time-averaged acetone PLIF image obtained during the run is shown in Fig. 5. The false coloring is applied to the acetone seeded primary (dark-brown) and secondary (pale-green) flow. They are overlapped one over the other to emphasize the aspects of flow mixing inside the supersonic confined jet. The presence of shock cells near the nozzle lip, growing mixing layer around the shock cell and the mixed flow with uniform scalar distribution far downstream the nozzle exit are clearly represented. Arbitrary locations of the L_{NM} and L_{PC} of the primary flow from the previous PLMS experiments of Karthick et al. (2016a) are also shown along with the L_{MIX} observed from the current acetone PLIF experiments. More details regarding the fluid physics and the jet characteristics will be discussed in Sec. 3 & 4.

2.3 Operating Conditions

As shown in Fig. 3, four different primary flow supersonic nozzle of design Mach numbers (M_{PD}) 1.5, 2.0, 2.5 and 3.0 are used to produce the primary supersonic jet at various conditions. Every nozzle is subjected to a range of primary flow stagnation pressures (P_{OP}) from 4.89 bar to 9.89 bar. The secondary air duct is fully opened to the ambient. Both the primary flow and the secondary flow use air as the working fluid. The stagnation temperature of both the fluids (T_{OP} & T_{OS}) is at ambient temperature (300 K). The ambient pressure (P_{amb}) observed during the experiment is 0.89 bar. Because of the above said conditions, during the operation of the supersonic confined jet, stagnation pressure ratio (SPR) of 6 to 13, compression ratio (CR) of 1.1 to 2.0, and entrainment ratio (ER) of 0.145 to 1.126 is achieved. Based upon the ratio of P_{OP} and the minimum wall static pressure (P_{min}) encountered in the constant area mixing duct, fully expanded primary jet Mach number (M_{PJ}) is defined from the isentrop-

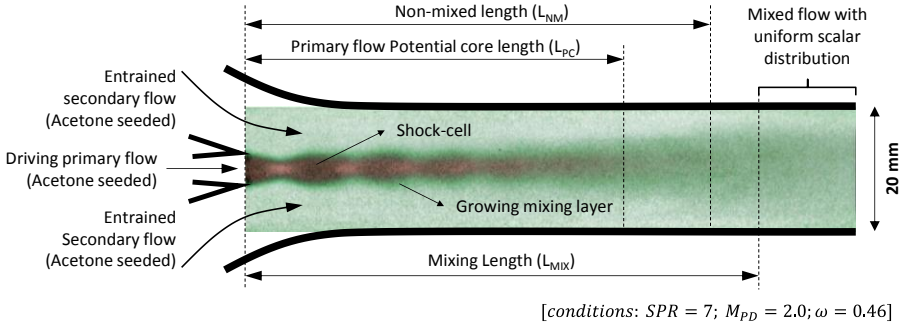

Fig. 5 Typical representation of a time-averaged acetone PLIF image showing the evolution of the confined supersonic jet and the associated flow features. False color representation is used for clarity. The primary flow acetone seeding is represented in dark-brown and the secondary flow acetone seeding is represented in pale-green

$$\frac{P_{OP}}{P_{min}} = \left(1 + \frac{\gamma - 1}{2} M_{PJ}^2\right)^{\left(\frac{\gamma}{\gamma-1}\right)} \quad (2)$$

$$h_J = h \frac{M_{PD}}{M_{PJ}} \left\{ \frac{1 + \frac{\gamma - 1}{2} M_{PJ}^2}{1 + \frac{\gamma - 1}{2} M_{PD}^2} \right\}^{\left(\frac{\gamma+1}{2(\gamma-1)}\right)} \quad (3)$$

$$Re_J = \frac{\rho_J u_J h_J}{\mu_J} \quad (4)$$

ic relations (Eq. 2). Using the mass conservation law (Tam and Tanna 1982; Tam 1988) between the M_{PD} and M_{PJ}, fully expanded primary jet height (h_J), velocity (u_J) and (ρ_J) is defined (Eq. 3). Viscosity values corresponding to the fully expanded jet Mach number (μ_J) are computed from Sutherland's formula ($\mu_0 = 1.827 \times 10^{-5}$ kg/m·s, $T_0 = 300$ K and C (air) = 120 K). The Reynolds number (Re_J) corresponding to the fully expanded conditions (Eq. 4) is in the range of 0.15 to 1.3 million. As mentioned in Karthick et al. (2016b) the fully expanded conditions are used as the scaling parameters for the representation of observed data. Based upon the nozzle pressure ratio ($NPR=P_{OP}/P_{ne}$), the primary nozzle can be operated at different conditions, ranging from the under-expanded nozzle to severely over-expanded nozzle. In order to represent the nozzle operating conditions, Mach number ratio (M_{PD}/M_{PJ}) is used as the non-dimensionalized parameter (Karthick et al. 2016c). [M_{PD}/M_{PJ}] will be unity if the nozzle is perfectly expanded (PE). It will be greater than unity for the over-expanded (OE) nozzle and lesser than unity for the under-expanded (UE) nozzle. For some OE conditions, the primary supersonic jet will be deviated (D) because of the flow separation (Shimshi et al. 2012) inside the nozzle. For the rest of the nozzle flow conditions, the primary supersonic jet is observed to be fairly centered (C).

3 Data Analysis

3.1 Wall Static Pressure

A typical runtime achieved during the operation of the supersonic confined jet is shown in Fig. 6 (conditions: SPR = 11.42; $M_{PD} = 1.5$; $\omega = 0.145$). The initial rise time of around 0.25 s is due to the opening of the rotary ball valve actuator, present after the pressure regulator (Fig. 2). After few milliseconds, the desired stagnation chamber pressure (P_{OP}) is reached. On an average, 2-3 seconds of steady runtime is achieved for the overall experimental matrix. All the corresponding data acquisition are carried out during this time, including wall static pressure measurements and acetone PLIF imaging. Each test case is repeated for at least five times for experimental consistency. Successive runs are carried out accordingly to acquire ample amount of data for statistical evaluation. This approach is especially helpful for acetone PLIF imaging, in case a deficiency is encountered in the total number of images required for time-averaging. Wall static pressure signals are acquired at 2 kHz. The acquired wall static pressure signals are raw and contain noise. A

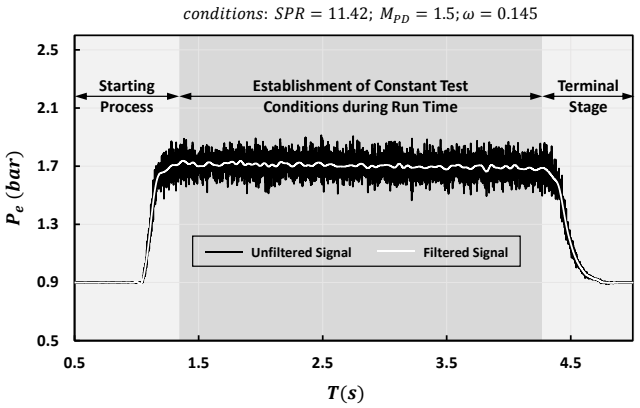

Fig. 6 Representation of typical run-time signal achieved (both unfiltered and filtered) during the operation of the supersonic confined jet by monitoring the exit pressure (P_e) near the diffuser end (conditions: SPR = 11.42; $M_{PD} = 1.5$; $\omega = 0.145$)

quick signal processing routine is used to overcome this difficulty. By using an in-house 'wavelet' filter, signal noises are eliminated. Both the raw and the filtered signals are represented clearly in Fig. 6. Wall static pressure is computed by taking the time-averaged pressure signal during the steady run-time. The net uncertainty involved in the wall static pressure measurements is about ±5% (Sec. 3.3). The final value is represented by taking the ensemble of the wall static pressures from the repeated runs of at least five times. The final values show a deviation less than 1% which is well within the uncertainty bound.

3.2 Acetone PLIF Image Analysis

3.2.1 Primary Flow Seeding & Secondary Flow Seeding

Acetone PLIF imaging is carried out by seeding the primary and the secondary flow individually with acetone vapors. Acetone vapors are the passive scalars introduced in the flow field. A typical normalized intensity profile observed along the centerline of the time-averaged acetone PLIF image for a particular flow condition is shown in Fig. 7. By examining the variation illustrated in Fig. 7, one can see that the intensity signals are weaker in the case of the primary flow seeding (shown in dotted line). On the other hand, by seeding the secondary flow, the intensity signals are stronger (shown in solid line). Acetone added into the primary flow stagnation chamber encounters a larger stagnation pressure compared with the acetone vapors added into the secondary stream which is at atmospheric pressure. In the recent works (Shelar et al. 2013; Shelar et al. 2014a), similar drop in fluorescence intensity has been observed with increase in tank pressure due to collisional transfer from acetone to triplet oxygen. Added to that, the low static temperature encountered in the supersonic primary jet can cause drop in the fluorescence intensity (Bryant et al. 2000). These might be the reasons for the low SNR encountered when the primary supersonic jet is seeded with acetone vapors. Nevertheless,

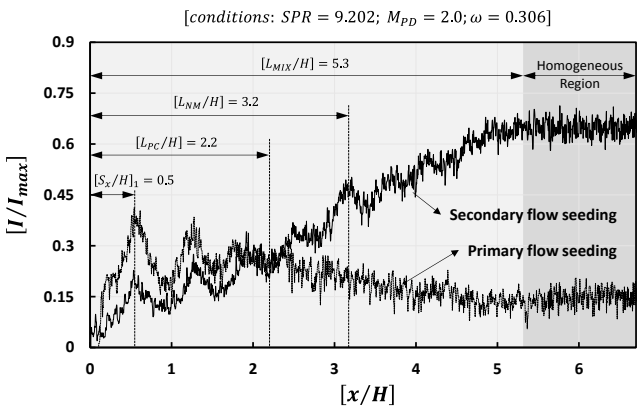

Fig. 7 Centerline intensity decay observed during the seeding of primary and secondary flow individually in the supersonic confined jet on the time-averaged acetone PLIF image (conditions: SPR = 9.202; M_{PD} = 2.0; ω = 0.306)

both methods of seeding mark the prominent flow features like the shock cell locations and the homogeneous region correctly, but with different level of intensity and SNR. Also, by making a keen observation in Fig. 7, one can see the occurrence of the homogeneous region remains the same, irrespective of the preferential flow seeding, except that the representation of such homogeneous region carries lesser uncertainty, if the secondary flow is seeded. While seeding the primary flow, it has to be noted that the low static temperature in the primary jet can cause acetone to condense, leading to non-conserved flow seeding. Given the case of current experimental matrix, the Mach 2 (M_{PD}) flow consists of both Perfectly Expanded (PE) and Under Expanded (UE) nozzle flow conditions, where the static temperature goes below 178.5 K (triple point of acetone). However, the major analysis in-terms of L_{MIX}, L_{PC} & S_x are determined from the acetone fluorescence images obtained by seeding the secondary flow alone, where the acetone vapors are seeded in the ambient conditions which is then entrained and mixed with the primary flow, downstream the L_{PC}. Typical values of secondary flow static temperatures encountered, for example in the case given in Fig. 11, is 280 K for the highest secondary flow Mach number (M_s = 0.4) encountered in the confined passage. These values are calculated based upon the wall static pressure distribution and the isentropic relationships. Apart from that, the numerical assessments carried out by Rao and Jagadeesh (2014), by solving the Navier-Stokes equations, the secondary flow static temperature for similar conditions can be found. Those values are also observed to be in the range as mentioned above. Hence, the entire set of experiments that are mentioned in this article are carried out by seeding the acetone vapors near the entrance of the entrainment duct into the secondary flow as represented in Fig. 2 to avoid unrealistic flow seeding and further errors in the calculation of respective parameters. It has to be noted that the authors are not trying to ascertain the exact concentration field inside the shock-laden near field of the primary supersonic jet which is an involved procedure. However, only the downstream characteristics of the mixed flow through the distribution of the fluorescent intensity from the passive scalar is determined in this article.

While seeding the secondary flow alone with the acetone vapors, the concentration of the acetone vapors can be selected using a simple procedure. The bubbling chamber is operated at a total pressure of 1.4 bar, constantly throughout the experiment. The total pressure is selected in such a way

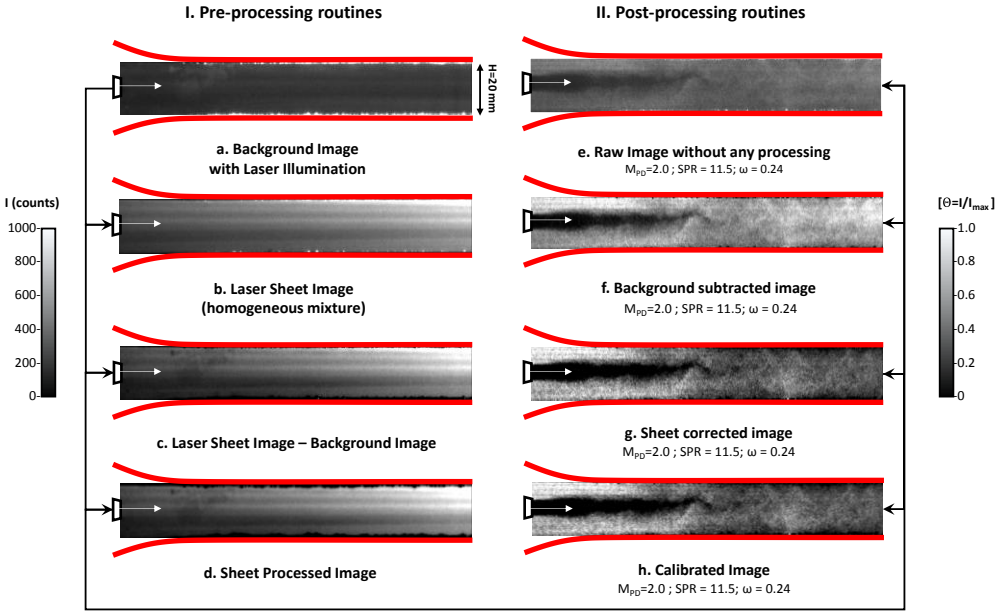

Fig. 8 Pre and post processing routines carried out on the acetone PLIF images which are obtained during the investigation of supersonic confined jets by seeding the secondary flow alone with acetone vapors (conditions: SPR = 11.5; M_{PD} = 2.0; ω = 0.24)

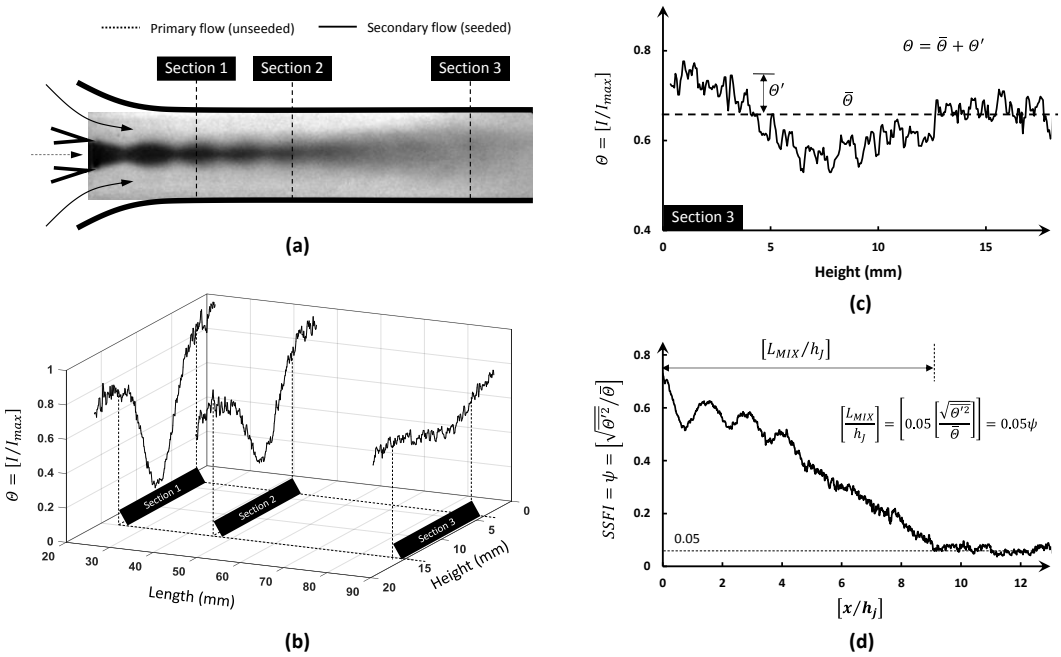

Fig. 9 Estimation procedure for mixed length (L_{MIX}) from the time-averaged acetone PLIF images. (a) A typical time-averaged acetone PLIF image acquired by seeding the secondary flow; (b) Normalized scalar profiles acquired at different transverse sections; (c) Observation of fluctuating scalar field in a given section; (d) Variations encountered in the Spatial Scalar Fluctuations Intensity (ψ) throughout the flow direction and the definition of L_{MIX}

that the flow through the bubbling chamber will not choke. It ensures homogeneous acetone vapor laden flow which contributes to 6 – 10% of the entrained mass through the secondary duct as the entrained flow is varying throughout the experiments based upon the operating conditions. Added to that, the obtained SNR is good enough for image analysis. In the work of Thurber and Hanson (2001), similar kind of acetone mass fraction has been already used in the heated subsonic turbulent jet in a weak co-flow studies, where air is the working fluid.

3.2.2 Image Pre & Post Processing Routines

Acetone PLIF images obtained for the quantification of L_{MIX} requires several mandatory pre and post processing routines. Most of these routines are well established in the literature (Vancruyningen et al. 1990; Gamba et al. 2015). Few important pre-processing routines like background subtraction, sheet correction, and sheet processing are carried out under standard conditions with and without acetone vapors. Severe parasite reflections and stray light reflections are often removed effectively from background subtraction routines, whereas the local laser sheet inhomogeneities due to the laser spatial profile and the associated noise in it are processed to perfection in the pre-processing routines of sheet correction and sheet processing. Nearly 50 images are taken and time-averaged for each pre-processing routine. For background subtraction, the flow field is captured under no flow conditions. For the sheet correction and sheet processing routines, the flow field is homogeneously seeded with acetone vapors under standard laboratory conditions. In order to simulate the static acetone vapor laden environment, the confined passage is isolated from the entry and exit air passages by means of a ball valve. After the sheet correction and sheet processing, flow field images are taken. Flow-field images during the test time are taken and the results from the pre-processing routines are then applied over those raw images during post-processing. Finally, the spatial calibration is imposed on the normalized acetone PLIF image. Typical steps involved in the acetone PLIF imaging is described in Fig. 8 clearly. Final images after the post-processing routines, consist of the planar concentration field, will be later used for further analysis.

3.2.3 Spatial Scalar Fluctuations Intensity (SSFI or ψ)

In the early studies of planar concentration field, apart from the centerline variation of concentration or concentration decay (Birch et al. 1984), few of the studies incorporated the idea of the dissipation rate (Markides and Mastorakos 2008; Stetsyuk et al. 2016) as one parameter to explore the varying concentration field, especially in the analysis of free jet (Vancruyningen et al. 1990) for larger distance. These studies are carried out mostly in incompressible free jets or far downstream of a compressible jet, where the effects of pressure and temperature is negligible. On the other hand, the shear layers are studied through the definition of shear layer growth rate (Papamoschou and Roshko 1988), which is the thickness of the visual shear layer formed between the two interacting fluids, either due to product formation (Clemens

and Mungal 1995) or through passive scalar marking (Su and Clemens 1999) of any one of the fluid. The former method is preferred to study the evolving structures inside the jet shear layer provided the field of investigation is larger along the jet propagating direction, and the later one is preferable to investigate the jet shear layer growth in the near-field. In the studies of a low area ratio supersonic confined jet, the second method is found to be an ideal candidate. Seeding any one of the fluid will help to track the shear layer growth and the fluid mixing to a better extent. We have already shown in Sec. 3.2.1 that in a dual stream mixing problem, seeding the subsonic stream with passive scalar has an added advantage, as it yields better SNR and less uncertainty. Also, in the recent literature (Takahashi et al. 2009), the analysis of successive transverse intensity profile variations along the flow direction of the acquired image has been proposed to study the confined jet characteristics effectively. In the recent works (Karthick et al. 2016a) of the authors, they have also employed similar techniques in the analysis of supersonic confined jet.

In this article, a method is proposed to represent the spatially varying fluctuating scalar field to study the mixing progression in a supersonic confined jet. The proposed method is similar to the degree of unmixedness quantified in the

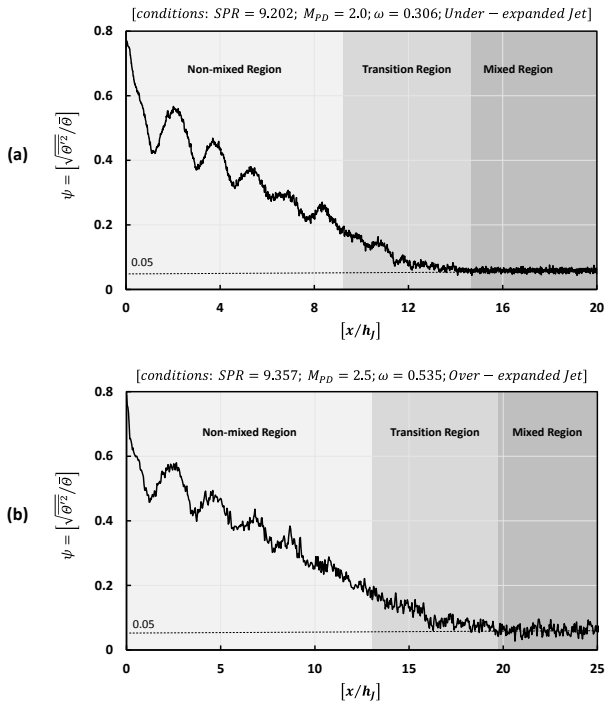

Fig. 10 Variations observed in the turbulent scalar intensity along the flow direction for different conditions. (a) Under-expanded supersonic primary jet (conditions: SPR = 9.202, M_{PD} = 2.0, ω = 0.306) (b) Over-expanded supersonic primary jet (conditions: SPR = 9.357, M_{PD} = 2.5, ω = 0.535). Three distinct regions are marked for clarity: Non-mixed Region (lighter gray), Transition Region (gray) and Mixed Region (Darker Gray)

$$SSFI = \psi = \sqrt{\overline{\theta'^2}}/\bar{\theta} \quad (5)$$

$$\theta = \bar{\theta} + \theta' \quad (6)$$

earlier literature (Dimotakis and Miller 1990; Fric 1993). However, even from the earlier days, researchers are giving different formulation for unmixedness, although they all use a combination of image statistics tool like average, sigma, variation of an image with a reference image etc. In this method, over the given planar scalar field, at every transverse sections, 'Spatial Scalar Fluctuations Intensity' (SSFI=ψ) is calculated. SSFI is defined as the ratio of the root mean square of the spatial scalar fluctuations ($\sqrt{\overline{\theta'^2}}$) to the mean sectional scalar variation ($\bar{\theta}$) in that section (Eq. 5). The definition of SSFI, helps in monitoring the homogeneity of the introduced scalar at every section for the given planar area of investigation. Typical observation of SSFI at different sections for a given planar flow field is shown clearly in Fig. 9. Three different sections are taken from the time averaged acetone PLIF image as shown in Fig. 9(a). The planar scalar field (θ) can be represented by taking the post processed acetone PLIF image and normalize the local intensity (I) with the maximum intensity (I_{max}) encountered in the planar field. In each transverse section, the variation of the local scalar field (θ) is plotted as shown in Fig. 9(b). At every transverse sections, the spatial fluctuations of the local scalar field (θ) can be represented as the sum of the mean scalar field ($\bar{\theta}$) in that section and the fluctuations of the scalar field (θ') from the mean (see Fig. 9 (c) & Eq. 6). At Section 1, the values are found to be maximum towards both the end of the section and the minimum values are found to be near the center (steeper curve). This indicates the presence of maximum acetone concentration in the secondary flow and the absence of acetone vapors in the primary flow. On looking at Section 2, it can be seen that the peak values of the secondary flow concentration is slightly lower and the minima is observed to be larger than the previous section, indicating the scalar transport from the secondary flow in to the primary flow (smooth curve). While looking at the concentration profile far downstream from the exit plane of the primary nozzle, the profile looks almost fuller, confirming the scalar equilibrium existing in the mixed flow. On marching further downstream, the shape and magnitude of the profile seldom changes, indicating the attainment of thorough scalar mixing.

3.2.4 Criterion for Mixed Length (L_{MIX})

After the definition of ψ at every transverse section in the planar scalar field, the variation of ψ along the flow direction is monitored, as it yields more information about the scalar mixing progression. On observing the variations of ψ in Fig. 9(d), one can see that the decreasing ψ values tend to rise at the mid-point of the shock cells and come down to a minimum between successive shock-cells in the near field of the primary supersonic jet. After the end of the potential core (L_{PC}) of the primary supersonic jet, such peaks are not observed and the values of ψ decay continuously. As we

Table 1 Table of experimental conditions for different primary flow design Mach numbers (M_{PD}). UE = under-expanded jet; OE = over-expanded jet; PE = perfectly expanded jet; C = centered jet; D = deviated jet;

Primary flow design Mach number (M_{PD})	Primary flow total pressure (P_{OP})	Nozzle pressure ratio (NPR)	Primary flow fully expanded jet Mach number (M_{PJ})	Effective primary jet height (h_J)	Mach number ratio (M_{PD}/M_{PJ})	Mixed length (L_{MIX}/h_J)	Nozzle Flow Condition & Direction
1.5	4.89	6.05	1.85	7.62	0.81	6.95	UE – C
	5.89	7.33	1.97	8.43	0.76	6.87	UE – C
	6.89	8.53	2.07	9.12	0.73	6.54	UE – C
	7.89	9.72	2.15	9.80	0.70	6.21	UE – C
	8.89	10.93	2.22	10.38	0.68	5.74	UE – C
	9.89	12.13	2.28	10.59	0.66	4.76	UE – C
2.0	4.89	6.21	1.88	5.42	1.07	19.06	OE – D
	5.89	7.48	2.00	6.01	1.00	18.53	PE – C
	6.89	8.60	2.09	6.47	0.96	17.03	UE – C
	7.89	9.67	2.16	6.87	0.93	14.79	UE – C
	8.89	10.81	2.23	7.30	0.90	11.42	UE – C
	9.89	12.04	2.30	7.77	0.87	10.57	UE – C
2.5	4.89	5.85	1.81	3.31	1.38	12.58	OE – D
	5.89	7.46	1.99	3.80	1.26	24.57	OE – D
	6.89	8.85	2.10	4.19	1.19	20.29	OE – C
	7.89	10.32	2.21	4.61	1.13	22.32	OE – C
	8.89	11.59	2.29	4.94	1.09	20.35	OE – C
	9.89	12.75	2.35	5.21	1.07	17.34	OE – C
3.0	4.89	6.01	1.82	2.07	1.65	16.05	OE – D
	5.89	7.42	1.96	2.31	1.53	31.53	OE – D
	6.89	8.49	2.06	2.52	1.45	29.82	OE – D
	7.89	10.27	2.20	2.85	1.36	26.95	OE – C
	8.89	11.73	2.29	3.07	1.31	26.39	OE – C
	9.89	13.20	2.37	3.30	1.27	28.01	OE – C

further proceed downstream, one can see that the ψ values start to plateau immediately after reaching a value of about 0.05 at certain x-location and it tends to remain almost invariant throughout the field of investigation. The distance along the flow direction at which the above said phenomenon occurs is defined as the 'mixed length (L_{MIX})'. For the definition of L_{MIX}, the authors find the definition of (ψ) more meaningful, as it maps the location of L_{MIX} consistently for all the conditions under study. Also, the values (specifically, L_{MIX}) obtained from the acetone PLIF images and the wall static pressure measurements (Fig. 11, Sec. 4.1) render this definition appropriate for the current studies. Since ψ is a non-dimensionalized parameter, the small variations in the mass fraction of the acetone vapors in the secondary flow (Sec. 3.2.1) will not influence the definition of L_{MIX}.

Typical variation in the ψ observed for two different conditions are shown in Fig. 10. In Fig. 10(a), a case of under-expanded primary supersonic jet is shown. In Fig. 10(b), a case of over-expanded primary supersonic jet of almost similar SPR is compared with the previous. In each case, the non-mixed length (L_{NM}) from the previous PLMS experiments (Karthick et al. 2016a) are marked for the reference. The region between the mixed and the non-mixed region is called as the transition region. All these areas are appropriately shaded to identify it visually. In both the cases, it is evidently seen that the ψ decays almost linearly after the termination of potential core (L_{PC}) of the primary supersonic jet and attains an invariant value of 0.05 further downstream. However, the location where a 5% in ψ is observed, is found to be different for both the cases. Discussions regarding this difference are described in detail in the upcoming sections (Sec. 4.2).

3.3 Uncertainty

All the measured quantities consist of inherent errors accumulated during the course of acquisition and calculation. They contribute to the overall uncertainty. For the statistical consistency, all the experiments are repeated at least five times, and the results are reported with the standard deviation from the mean. Representation of stagnation pressures (P_{OP} and P_{OS}) and exit pressure (P_e) using IRA gauges contribute to the overall uncertainty of about ±2% from the measured values. Representation of primary and secondary mass flow rates using the venturi meter arrangement near the exit of the supersonic confined jet passage and the entrance of the secondary air-intake duct contribute to the overall uncertainty of about ±5% from the measured values. Using the Freescale™ MPX pressure transducers, the wall static pressures are measured with the overall uncertainty of ±5% from the

measured values. Following the procedure prescribed in Rao and Jagadeesh (2014) for the measurement of L_{NM} and Karthick et al. (2016a) for the measurement of L_{PC}, the values of L_{PC} discussed for particular flow conditions are estimated to carry an uncertainty of ±7% from the measured values. The estimated scalar field using the acetone PLIF imaging procedures have an uncertainty of ±5% from the measured values. Determination of L_{MIX} from the above imaging technique and using the processing procedure as elaborated in Sec. 3.2.4, carries an overall uncertainty of ±7% from the measured values. The extent of uncertainty mentioned above for every measurement, include the errors in the acquisition devices (<1%) and the pre/post processing routines (<1%).

4 Observations and discussions

In this section, observations from the acetone PLIF experiments are discussed briefly in four parts. The first section contains the observations from the wall static pressure measurements. In the second section, variations observed in the L_{MIX} for different operating conditions are discussed. The third section carries the L_{PC} results from acetone PLIF imaging. The variation of L_{PC} between free and confined jet is highlighted for the selected case. Similar to the previous section, in the fourth section, shock cell spacing [S_x] is calculated from acetone PLIF imaging. In Table 1, experimental conditions along with the L_{MIX} findings are specifically given. It is important to tabulate few of the performance parameters of the supersonic confined jet, as they are dependent and sensitive to geometrical changes and the operating conditions. During the experiments, the primary jet is found to be deviating (D) from the centerline in few cases due to an earlier asymmetric separation (Shimshi et al. 2012) inside the CD nozzle. They are mostly encountered in over-expanded (OE) CD nozzles. Those cases are avoided in the further discussions, and the values L_{MIX}, L_{PC} and S_x for such conditions are not represented here. Apart from the severely over-expanded (OE) nozzle conditions, for other under-expanded (UE), perfectly-expanded (PE) and moderately over-expanded cases, the primary supersonic jet is observed to be centered (C). In the upcoming sections, those cases are only considered for the discussions.

4.1 Wall Static Pressure Distribution

Variations observed in the wall static pressure measurements shed valuable information regarding the gaseous mixing process to a certain extent. A typical wall static pressure variation in a supersonic confined jet is shown in Fig. 11 (conditions: SPR = 7.481; M_{PD} = 2.0; ω = 0.445). A linear drop in pressure as shown in Fig. 11, between [x/H] of -4 to 0, represents the acceleration of secondary gas entering into the constant area mixing duct from the secondary flow stagnation chamber. The expanding jet from the primary supersonic jet nozzle (for the case shown in Fig. 11, the primary supersonic jet nozzle is under-expanded) offers narrow passage to the entrained flow because of the growing mixing layer. This, in turn, accelerates the secondary flow rapidly at that particular location causing local minima (x/H≈1 in Fig. 11) in the wall static pressure measurements (P_{min}). The mixing layer from the primary supersonic jet continues to thicken, thereby entraining more fluid into the mainstream. A gradual pressure rise observed between [x/H] of 2 to 4 in Fig. 11 represents the above said physics. Till this region, the supersonic confined jet retains its distinct characteristics, and the length is identified as non-mixed length (L_{NM}) in the previous work of the authors (Rao and Jagadeesh 2014; Karthick et al. 2016a). The thickening mixing layer then interacts with the surrounding wall or due to jet column instability (Moreno et al. 2004) it breaks down to small structures, thus leading into rapid turbulent fluid mixing. During this process of turbulent mixing, a considerable amount of energy from the flow is taken and the receding flow causes a local pressure rise. This can be evidently seen in Fig. 11, between [x/H] of 5 to 6.5. Complete passive scalar mixing is expected around this region. Even, the calculated L_{MIX} through the

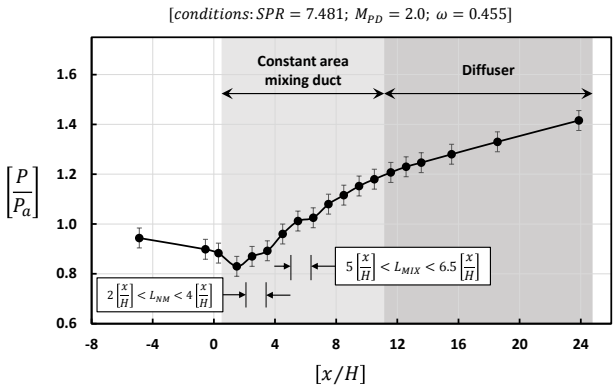

Fig. 11 A typical variation of the wall static pressures observed in the center plane (z=0) of a supersonic confined jet (conditions: SPR = 7.481; M_{PD} = 2.0; ω = 0.445). A Lighter gray area marks the region of constant area mixing duct, and a darker gray area marks the region of the diffuser

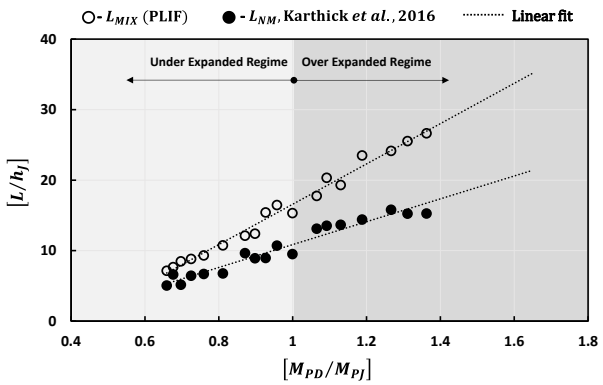

Fig. 12 Variation observed between the mixing length (L_{MIX}) and the non-mixed length (L_{NM}) for different operating conditions of the primary supersonic jet through the definition of Mach number Ratio (M_{PD}/M_{PJ})

method given in Sec. 3.2.4 yields a value of [L_{MIX}/H]=5.6, which lies in the same region marked by the wall static pressure measurements. After that, the gradual pressure rises up to [x/H] of 11 is due to shear forces or wall. From there onwards (11 <[x/H] <24), the connected diffuser recovers the pressure further downstream which can be evidently seen at P_e which is larger than the atmospheric pressure. Spatial resolution in the sensor placement is found to be poor which limits us from measuring the precise location of L_{MIX}.

4.2 On the Observation of Mixing Length (L_{MIX})

After extracting the scalar profiles through the methodology as detailed in Sec. 3.2.2, definitions are formulated (Sec. 3.2.4) to quantify the mixing length (L_{MIX}) in the supersonic confined jet. As the observed scalar field is bounded by the surrounding wall, it is much easier to infer the scalar variations across every transverse section. Nevertheless, an appropriate method is required to quantify the L_{MIX} and the introduction of ψ solves that problem. Comprehensive observation of L_{MIX} which is obtained through the procedures described in Sec. 3.2.4 for different operating conditions through the representation of Mach number ratio (M_{PD}/M_{PJ}) is given in Fig. 12. The values of the L_{MIX} are scaled using the fully-expanded jet height (h_J) as described in the earlier section (Sec. 2.3). From Fig. 12, it can be seen that there exist a linear variation in the observed trend. Hence a linear model through Eq. 9 is applied to the acquired data with a goodness fit (R^2) of 0.9834. By decoupling the values of L_{MIX} from Eq. 7 and by substituting the values of h_J, the in-

$$\left[\frac{L_{MIX}}{h_J}\right] = A_1\left[\frac{M_{PD}}{M_{PJ}}\right] + A_2\left[\frac{W}{w}\right]\left[\frac{H}{h}\right] \qquad \begin{matrix} A_1 = 28.57; \\ A_2 = -3.37; \end{matrix} \qquad (7)$$

fluences of the nozzle operating conditions on the mixing process can be studied. By doing so, the L_{MIX} observed from the acetone PLIF experiments for the under-expanded supersonic primary jet is found to be larger than that of the over-expanded supersonic primary jet, just as observed from the previous experiments (Karthick et al. 2016a) of L_{NM} through PLMS. To the maximum of 17.67% reduction in L_{MIX} is observed when the primary supersonic jet is over-expanded instead of perfectly expanded. On the other hand, a maximum increment of 15.76% in the L_{MIX} is seen when the primary supersonic jet is under-expanded instead of perfectly expanded. The variation is due to the higher kinetic energy contained in the primary supersonic jet (ρu_J^2) at lower Mach number ratio. These arguments seem to be consistent with the previous findings of the L_{NM}. Although, upon comparing the values of L_{NM} and L_{MIX}, both the values are found to be nearer for the under-expanded case and are observed to be farther for the over-expanded case (see Fig. 12). Also, the slope of the linear fit in the case of L_{MIX} is found to 80% larger than the L_{NM}. It is expected that L_{MIX} will be further downstream from the L_{NM}, as the decelerating jet will take certain length to disintegrate and engage in turbulent mixing.

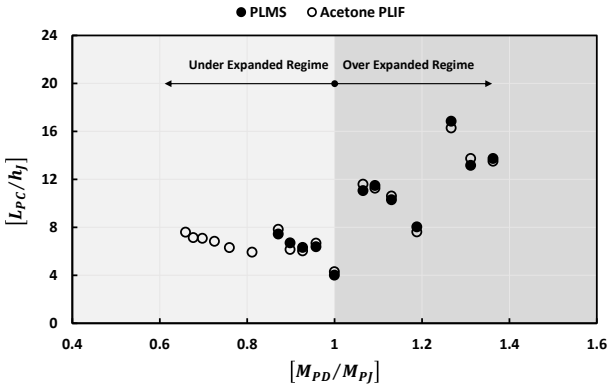

Fig. 13 Variation in the potential core length (L_{PC}) of the primary supersonic jet in the supersonic confined jet for various operating condition through the definition of Mach number ratio [M_{PD}/M_{PJ}] using techniques like Planar Mie Scattering (PLMS) and acetone Planar Laser Induced Fluorescence (PLIF). Lighter gray region marks the regime of the under-expanded primary supersonic jet and the darker gray region marks the regime of the over-expanded primary supersonic jet

The closer values that are observed in the under-expanded region on Fig. 11 and the larger deviations encountered in the L_{MIX} observations from the L_{NM} at the over-expanded nozzle flow conditions lead to further investigations. To explore the flow physics, entrainment ratio (ER) calculated by measuring the ratio of the mass flow rate of the entraining fluid ($\dot{m}_s$) and the primary fluid ($\dot{m}_p$) through pressure measurements are considered. For a similar SPR conditions (SPR≈9.2), one of the under-expanded (M_{PD}=2.0; ω=0.306) and the over-expanded (M_{PD}=2.5; ω=0.535) jets are examined. Looking at the ER values for the under-expanded primary jet, they are observed to be smaller. Because the flow is under-expanded, h_J is greater than the nozzle exit height and, it offers narrow flow passage for the secondary stream, thereby limiting the secondary mass flow rate. The lower secondary flow entrainment leads to quicker mixing with the primary flow which leads to the shorter L_{MIX}. Also, for some of the under-expanded cases, especially for M_{PD}=1.5, the values of h_J goes to a maximum of 50% of the mixing duct height (H). This behavior of the under-expanded jet makes the evolving mixing layer interact with the bounding wall quickly rather than the over expanded case, despite the lower mixing layer growth rate. This rapid interaction of the mixing layer with the surrounding wall premature the process of jet disintegration and enhances the mixing of primary and the secondary fluid. Because of these reasons, L_{NM} from the PLMS experiments and L_{MIX} from the acetone PLIF experiments are closer for the under-expanded nozzle flows.

As the duct height is only 20 mm at the constant area duct portion, it renders other measurement techniques obsolete to estimate the boundary layer thickness near the top or bottom wall of the confined passage. Irrespective of that, from the work of Stratford and Beavers (1959), boundary layer thickness under arbitrary pressure gradients can be estimated using simple correlations. Using those correlations, the typical value of the boundary layer thickness is found to be 0.6 mm.

The calculation is carried out at the top or bottom wall which is located 40 mm (2H) downstream from the nozzle exit plane, for the conditions given in Fig. 11. The values are in agreement with the numerical assessments of Rao and Jagadeesh (2014) in the rectangular supersonic gaseous ejector, under similar flow conditions. Since, the values of the incoming boundary layer thickness is negligible in the entry section, its influence on the L_{MIX} is only minimal.

4.3 Potential core length (L_{PC}) of the primary supersonic jet

Potential core studies pave another way in the understanding of mixing process in the supersonic confined jet. The extent of the L_{PC} gives information regarding the non-mixed portion in the mixing duct. The developing mixing layer from either side of the primary nozzle lip moves towards the jet axis and marks the termination of the potential core length (L_{PC}) of the primary supersonic jet. In the previous PLMS studies (Karthick et al. 2016a), potential core (L_{PC}) variations in the primary supersonic jet are shown for selected case. The main reason for the presentation of particular cases is because the primary flow is self-seeding due to severe nucleation (Ding et al. 2014b; Ding et al. 2014a) happening inside the nozzle. This in-turn prevents the seeding of secondary flow alone to visualize the potential core. This phenomenon is seen consistently in all the cases of M_{PD}=1.5. In the current experimental matrix, cases of M_{PD}=1.5 represent the severely under-expanded nozzle flows. Comprehensive discussions on the L_{PC} of the primary jet was limited in previous experiments (Rao and Jagadeesh 2014; Karthick et al. 2016a). In the current experimental technique, effects of the nucleation can be eliminated from the final image, as the final image contains only the fluorescence signal coming from the acetone seeded secondary flow but not from the self-seeding primary flow. Also by adopting the similar image analysis routines prescribed in the previous work, L_{PC} calculation using the acetone PLIF technique compliments the previous experimental results from PLMS methods. In Fig. 13, the variation of L_{PC} observed through PLMS and acetone PLIF imaging techniques for different operating conditions are given. The maximum variations in the calculated L_{PC} between both the experiments are less than 7% which is well within the uncertainty limit of these techniques. The similarity in the magnitude and the trend shows the reliability of the experimental methods and the inferences. Fig. 14, gives a general observation of primary flow L_{PC}, non-dimensionalized with fully expanded jet height or effective jet height (h_J) for different Mach number ratio (M_{PD}/M_{PJ}). The plot consists of the variations observed experimentally using acetone PLIF technique in the case of the supersonic free jet and the supersonic confined jet for comparison. The acquired values are also plotted against the findings of Lau et al. (1979) as mentioned in Eq. 8 for comparison. It has to be noted that the component D_J is the equivalent hydraulic jet diameter if the nozzle under study is planar. While representing in the graph as shown in Fig. 14, the values are rescaled based upon h_J. It has to be noted that the equation considers flows that are under-expanded alone, as the relation was derived from a sonic nozzle whose operational regime was only in the under-expanded regime. Because of that, cases of M_{PD}=1.5 lies close to the theoretical estimates by ±5% for the selected case of moderately under-expanded supersonic free jet experiments (M_{PD}/M_{PJ} < 0.75). However, the equation does not predict the variations for severely under-expanded and also for severely over-expanded conditions (not shown in Fig. 14 for clarity). Even in the current case, for higher M_{PJ}, marked by lower Mach number ratio, the values are off by a maximum of 15%. Many reasons are attributed to the observed variation in a planar CD nozzle. Recent work of Heeb et al. (2014) argues that the acoustical effect of the supersonic jet, primarily due to 'screeching' might be one reason. However, compared with the supersonic confined jet, the L_{PC} of the supersonic free jet is observed to be far higher. However, for higher M_{PJ}, there is no evidence of such screeching phenomena (Tam 1988). The possible reason for this discrepancy is due to core turbulence (Raman and Rice 1993) effect and the jet column's self-sustained oscillation (Moreno et al. 2004) as reported earlier in the literature. Destabilization and reduction of the potential supersonic core are well-known phenomena when the incoming turbulence levels are high (Franquet et al. 2015). This in-turn makes the mixing layer to thicken and diminishes the supersonic potential core. Looking at the variations in case of the supersonic confined jets, the observed L_{PC} are far below the supersonic free jet case. In the event of a free jet, the streamlines dive into the jet shear layer from the surroundings, contributing a higher convective Mach number (M_c). On the other hand, the co-flowing streamlines observed in a confined jet, run along with the primary supersonic jet and produces lower M_c, comparative-

$$\left[\frac{L_{PC}}{D_J}\right] = a + b\,M_{PJ}^2, \quad where\ a = 4.2\ and\ b = 1.1 \tag{8}$$

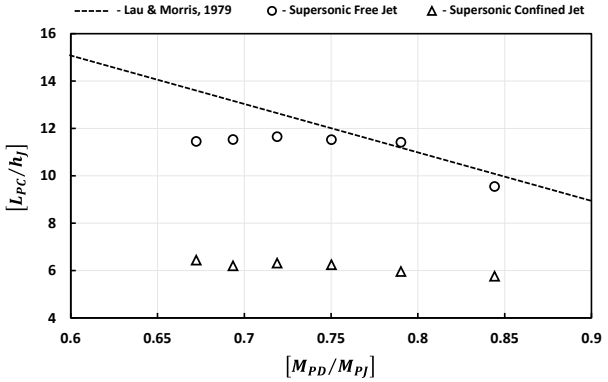

Fig. 14 Variation of potential core length of the primary supersonic jet at different conditions through the definition of Mach number ratio (M_{PD}/M_{PJ}) for the primary nozzle of design Mach number M_{PD} = 1.5. The graph depicts the variations seen between the supersonic free jet, both experiment (circle) & theory (dash line), and supersonic confined jet (experiment-triangle)

ly. Observation of lower M_c in the supersonic confined jet tends to increase the L_{PC}, as the flow ingest or entrain smaller amount of fluid. However, as said in the previous sections (Sec. 4.2), the severely under-expanded jets interact with the wall very quickly upon expansion and diminishes the potential core in the earlier stage itself. This once again supplements the observation of lower L_{PC} in the supersonic confined jets compared with the supersonic free jet.

4.4 Shock-cell Spacing

An important characteristic of the supersonic jet is the shock-cell spacing (Franquet et al. 2015). Shock cell spacing in a supersonic free jet, both circular and planar jet are verified experimentally and theoretically in previous literature (Franquet et al. 2015). Theoretical estimation of shock cell spacing by Norum and Seiner (1982) as shown in Eq. 9, is used here to compare and contrast the jet morphology of a supersonic confined jet from the supersonic free jet.

$$\left[\frac{S_x}{D_J}\right]_1 = c\left(M_{PJ}^2 - 1\right)^{d/2}, \ \ where\ c = 1.1\ and\ d = 1.17 \qquad (9)$$

A recent attempt in mapping the shock wavelength has been made by Zhu and Jiang (2014), using the Schlieren experiments for a slightly different area ratio and operating conditions than the experimental setup considered here. They have shown a comparable match with Tam's (Tam and Tanna 1982; Tam 1988) observation. However, for the supersonic confined jets of lower area ratio operating in the mixed regime (Dutton et al. 1982), there has been no reports on shock cell spacing. From the methodology adopted in the estimation of L_{MIX} through the definition of ψ, shock cell spacing can also be deduced easily. As the ψ calculations are the sectional intensity scans throughout the flow passage, while seeding the secondary flow, the estimates as shown in Fig. 10 marks the position of shock cells through peaks and valleys. Every valley points seen in the graphical representation of Fig. 10 from the nozzle exit, corresponds to the terminal location of a shock cell. Typically, three to four shock cells can be easily identified by monitoring the variation of ψ throughout the mixing duct for the given experimental matrix. The bumps seen in the ψ variations vanish and decay linearly once the mixing layer thickens and the potential core of the primary flow terminates. The physical feature of the shock cells obviously terminates before the potential core end or the sonic line as shown in the schematic (Fig. 1). Plotting the variation of successive shock cell spacing (S_x) through a non-dimensionalized parameter h_J helps in understanding the supersonic confined jet behavior clearly. In Fig. 15, successive shock cell spacing (up to 3 shock cell locations) are plotted for the primary nozzle whose design Mach number (M_{PD}) is 2.0. The specific case has been chosen because it contains all the nozzle flow conditions. It can be seen from the graph that the first shock cell of an over-expanded supersonic confined jet is off by almost 56% compared with the supersonic free jet case. Later, when M_{PJ} rises,

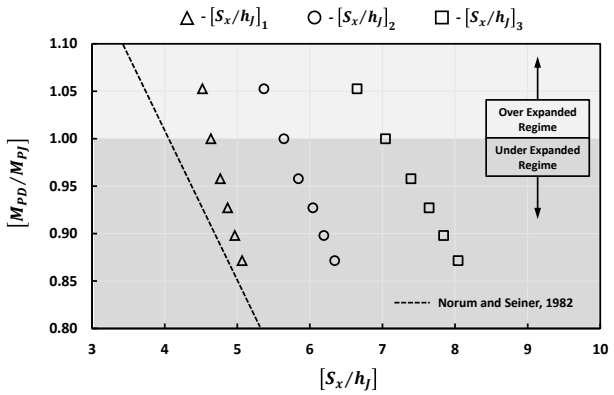

Fig. 15 Variations observed in the successive shock cell spacing for different nozzle operating conditions through the definition of Mach number ratio for the primary nozzle of design Mach number M_{PD} = 1.5. Values are compared with previous data of Norum and Seiner, 1982 (dashed lines). Shock cell location markings: First cell – triangle; Second cell – circle; Third cell – square;

the difference observed between the first shock cell of the confined jet and the free jet decreases, gradually. Once again, a lower amount of fluid entrainment and the presence of similar static pressure around the primary jet, as observed in the free jet, might be the reason. However, the distance between successive shock cell spacing starts to increase as M_{PJ} increases. This clearly indicates the influence of the surrounding wall and the kinetic energy of the primary jet (ρu_J^2). This behavior is evidently seen at the highest M_{PJ} observed for M_{PD}=2.0, where the successive shock cell spacing has increased almost by 75% between the first $[S_x]_1$ and the second $[S_x]_2$ shock cell. Similarly, an increment by 30% can be seen between the second $[S_x]_2$ and the third $[S_x]_3$ shock cell. When the flow under-expands inside the confined passage, it offers constriction to the entraining fluid. The accelerating fluid through the constrained passage and the growing mixing layer tends to increase the shock cell width. Also, while looking closer, the spacing of the shock cell increases between the second and the third almost by two times when compared with the first shock cell. From the wall static pressure measurements, as shown in Fig. 11, minimum wall static pressure (P_{min}) also occurs in this region. Despite all these happenings, on looking into the gross variation of each shock cell, the variations seem to follow the same increasing trend as reported by Norum and Seiner (1982), but with different magnitude. To give a proper variation as observed in the

$$\left[\frac{S_x}{h_J}\right]_n = a_n\left[\frac{M_{PD}}{M_{PJ}}\right] + b_n \qquad (10)$$

Table 2 Coefficient values for the experimental curve fit

n	a_n	b_n
1	7.719	−3.064
2	11.045	−5.402
3	14.809	−7.751

current experimental case, following linear fit is proposed with an R^2 value of 0.99 as shown in Eq. 10 and Table 2, where *n* represents the shock cell number.

5 Conclusions

Detailed passive scalar mixing studies are carried out in a supersonic confined jet using acetone PLIF technique to identify the L_{MIX}. The primary supersonic jet is operated at four different M_{PD} of 1.5, 2.0, 2.5 & 3.0 at various P_{OP}, ranging from 4.89 bar to 9.89 bar. Following are the major conclusions drawn from the analysis of the experimental results:

1. Calculation of Spatial Scalar Fluctuations Intensity (ψ) by seeding the secondary flow alone is found to be useful in identifying the L_{MIX}. The first occurrence of ψ=0.05 in the given planar scalar field is set as a criterion for L_{MIX}.
2. Similar to the L_{NM} variations, the L_{MIX} variations are also found to be linear but with a higher slope of almost 80%. For certain operating conditions, the values of L_{MIX} are found to be reduced to a maximum of 17.67% for the over-expanded nozzle flows and increases to a maximum of 15.76% for the under-expanded nozzle flows.
3. Comprehensive L_{PC} measurements are made in this study which is not limited by self-nucleation effects. Severely under-expanded cases of M_{PD}=1.5 are observed in this study and L_{PC} is found to be invariant due to the rapid interaction of the primary jet with the surrounding wall.
4. Spacing of the successive shock cells $[S_x]_n$ vary linearly when the jet operating conditions change from over-expanded to under-expanded. The shock cell spacing is observed to be two times greater at the location where the minimum passage to the secondary flow is encountered. The variations in shock cell spacing of supersonic confined jet are found to be larger than the free jet case.

Acknowledgement

The authors would like to sincerely acknowledge the research grants (Grant No. DRDO 0626) from the Defence Research and Development Organization (DRDO), India. The authors would like to thank Dr. Vikas M. Shelar, Dr. Bindu, and Dr. Yedhu for their valuable inputs in the analysis of experimental results. The authors would also like to thank the research students in LHSR, especially Mr. Kannan Munusamy, Mr. Sneh Deep and Mr. G. Yogeshwaran for their timely help in setting up and conducting the experiments. Technical assistance offered by the LaVision support team specifically Mr. Arun and the expertise from Tesscorn Aerofluid Inc., chiefly Mr. Satyanarayana are duly acknowledged.

Appendix

Notations and definitions

PLIF	Planar Laser Induced Fluorescence
SNR	Signal to Noise Ratio
ICCD	Intensified Charge-Coupled Device
SSFI	Spatial Scalar Fluctuations Intensity
P_{OP}	Primary flow stagnation pressure (bar)
P_{OS}	Secondary flow stagnation pressure (bar)
T_{OP}	Primary flow stagnation temperature (K)
T_{OS}	Secondary flow stagnation temperature (K)
P_e	Mixed flow exit pressure (bar)
P_{min}	Minimum pressure encountered at the top wall of the mixing duct (bar)
P_{ne}	Pressure near the primary flow nozzle exit (bar)
P_a	Pressure in the ambient conditions (bar)
$\dot{m}_p$	Primary mass flow rate (kg/s)
$\dot{m}_s$	Secondary flow mass flow rate (kg/s)
SPR	Stagnation Pressure Ratio (P_{OP}/P_{OS})
CR	Compression Ratio (P_e/P_{OS})
NPR	Nozzle Pressure Ratio (P_{OP}/P_{ne})
ER or ω	Entrainment Ratio $(\dot{m}_s/\dot{m}_p)$
L_{PC}	Length of the primary flow potential core (mm)
L_{NM}	Non-mixed length from PLMS experiments (mm)
L_{MIX}	Mixed length from acetone PLIF experiments (mm)
M_{PD}	Design Mach number of the primary nozzle
M_{PJ}	Fully expanded jet Mach number issuing from primary nozzle
M_{PD}/M_{PJ}	Mach number ratio
M_c	Convective Mach number
M_s	Secondary flow Mach number
AR	Area Ratio of the supersonic confined jet $[(W/w)\cdot(H/h)]$
W	Width of the mixing duct (mm)
w	Width of the primary flow convergent-divergent (CD) nozzle (mm)
H	Height of the constant area mixing duct in the supersonic confined jet (mm)
h	Height of the primary flow CD nozzle (mm)
μ	Dynamic viscosity of the fluid (kg/m·s)
Re_J	Reynolds number corresponding to fully expanded primary jet conditions $[\rho_J u_J h_J/\mu_J]$
h_J	Fully-expanded primary jet height (mm)
D_J	Equivalent hydraulic jet diameter (mm) $[(4Wh_J)/(2W+h_J)]$
u_J	Fully-expanded primary jet velocity (m/s)
ρ_J	Fully-expanded primary jet density (kg/m^3)
β_{mix}	Mixing parameter used in the definition of L_{NM} and L_{PC}
$[S_x]_n$	Successive shock cell spacing along x-direction (mm)
n	Shock cell number
ψ	Spatial scalar fluctuations intensity
θ	Normalized local scalar quantity (I/I_{max})
$\bar{\theta}$	Time-averaged scalar quantity
θ'	Fluctuating scalar quantity

References

Ariafar K, Buttsworth D, Sharifi N, Malpress R (2014) Ejector primary nozzle steam condensation: Area ratio effects and mixing layer development. Appl Therm Eng 71:519-527

Birch AD, Brown DR, Dodson MG, Swaffield F (1984) The Structure and Concentration Decay of High-Pressure Jets of Natural-Gas. Combust Sci Technol 36:249-261

Brehm C, Housman JA, Kiris CC (2016) Noise generation mechanisms for a supersonic jet impinging on an inclined plate. J Fluid Mech 797:802-850

Bryant RA, Donbar JM, Driscoll JF (2000) Acetone laser induced fluorescence for low pressure/low temperature flow visualization. Exp Fluids 28:471-476

Chen J, Wang ZG, Wu JP, Xu WW (2015) Investigation on the Pressure Matching Performance of the Constant Area Supersonic-Supersonic Ejector. Therm Sci 19:631-643

Chong DT, Hu MQ, Chen WX, Wang JS, Liu JP, Yan JJ (2014) Experimental and numerical analysis of supersonic air ejector. Appl Energy 130:679-684

Chunnanond K, Aphornratana S (2004) An experimental investigation of a steam ejector refrigerator: the analysis of the pressure profile along the ejector. Appl Therm Eng 24:311-322

Clemens NT, Mungal MG (1995) Large-Scale Structure and Entrainment in the Supersonic Mixing Layer. J Fluid Mech 284:171-216

Danckwerts PV (1952) The Definition and Measurement of Some Characteristics of Mixtures. Appl Sci Res 3:279-296

Desevaux P, Hostache G, Jacquet P (1994) Static pressure measurement along the centerline of an induced flow ejector. Exp Fluids 16:289-291

Desikan SLN, Saravanan R, Subramanian S, Sivararamakrishnan AE, Pandian S (2015) Investigation of Supersonic Jet Interaction With Hypersonic Cross Flow. J Fluid Eng-T Asme 137

Dimotakis PE, Miller PL (1990) Some Consequences of the Boundedness of Scalar Fluctuations. Phys Fluids a-Fluid 2:1919-1920

Ding HB, Wang C, Chen C (2014a) Non-equilibrium condensation of water vapor in sonic nozzle. Appl Therm Eng 71:324-334

Ding HB, Wang C, Chen C (2014b) Non-equilibrium condensation process of water vapor in moist air expansion through a sonic nozzle. Flow Meas Instrum 40:238-246

Dutton JC, Mikkelsen CD, Addy AL (1982) A Theoretical and Experimental Investigation of the Constant Area, Supersonic-Supersonic Ejector. AIAA J 20:1392-1400

Dvorak V, Safarik P (2003) Supersonic Flow Structure in the Entrance Part of a Mixing Chamber of 2D Model Ejector. J Therm Sci 12:344-349

Franquet E, Perrier V, Gibout S, Bruel P (2015) Free underexpanded jets in a quiescent medium: A review. Prog Aerosp Sci 77:25-53

Fric TF (1993) Effects of Fuel-Air Unmixedness on Nox Emissions. J Propul Power 9:708-713

Gamba M, Miller VA, Mungal MG, Hanson RK (2015) Temperature and number density measurement in non-uniform supersonic flowfields undergoing mixing using toluene PLIF thermometry. Appl Phys B-Lasers O 120:285-304

Handa T, Masuda M, Kashitani M, Yamaguchi Y (2011) Measurement of number densities in supersonic flows using a method based on laser-induced acetone fluorescence. Exp Fluids 50:1685-1694

Heeb N, Gutmark E, Kailasanath K (2014) An experimental investigation of the flow dynamics of streamwise vortices of various strengths interacting with a supersonic jet. Phys Fluids 26

Heiser WH (2010) Ejector Thrust Augmentation. J Propul Power 26:1325-1330

Houwing AFP, Palmer JL, Thurber MC, Wehe SD, Hanson RK, Boyce RR (1996) Comparison of planar fluorescence measurements and computational modeling of shock-layer flow. AIAA J 34:470-477

Karthick SK, Rao SMV, Jagadeesh G, Reddy KPJ Effect of Primary Flow Mach Number on the Non-Mixed Length in a Two Dimensional Supersonic Ejector. In: 30th International Symposium on Shock Waves, Tel-Aviv, Israel, 19-24, July 2015a. p 6

Karthick SK, Rao SMV, Jagadeesh G, Reddy KPJ (2015) Visualizing the flow through a supersonic gaseous ejector using Planar Laser Mie Scattering. In: 10th Pacific Symposium on Flow Visualization and Image Processing, Naples, Italy, 15-18, June 2015b. Italy, Naples, p 8

Karthick SK, Rao SMV, Jagadeesh G, Reddy KPJ (2016a) Parametric Experimental Studies on Mixing Characteristics within a Low Area Ratio Rectangular Supersonic Gaseous Ejector. Phys Fluids 28

Karthick SK, Rao SMV, Jagadeesh G, Reddy KPJ Scaling and non-dimensionalization studies on mixing characteristics within a rectangular supersonic gaseous ejector. In: National Shock Waves Symposium (NSSW 4, Coimbatore, India, 2016b.

Karthick SK, Shelar VM, Jagadeesh G, Reddy KPJ Studies on mixing in the supersonic gaseous ejector using acetone PLIF. In: National Shock Waves Symposium (NSSW 4), Coimbatore, India, 2016c.

Kracik J, Dvorak V, Kolar J (2014) Development of air to air ejector for supersonic wind tunnel. EPJ Web Conf 67:2

Lau JC, Morris PJ, Fisher MJ (1979) Measurements in Subsonic and Supersonic Free Jets Using a Laser Velocimeter. J Fluid Mech 93:1-27

Lozano A, Yip B, Hanson RK (1992) Acetone - a Tracer for Concentration Measurements in Gaseous Flows by Planar Laser-Induced Fluorescence. Exp Fluids 13:369-376

Markides CN, Mastorakos E (2008) Measurements of the statistical distribution of the scalar dissipation rate in turbulent axisymmetric plumes. Flow Turbul Combust 81:221-234

Mazzelli F, Milazzo A (2015) Performance analysis of a supersonic ejector cycle working with R245fa. Int J Refrig 49:79-92

Moreno D, Krothapalli A, Alkislar MB, Lourenco LM (2004) Low-dimensional model of a supersonic rectangular jet. Phys Rev E 69

Norum TD, Seiner JM (1982) Broad-Band Shock Noise from Supersonic Jets. AIAA J 20:68-73

Papamoschou D, Roshko A (1988) The Compressible Turbulent Shear-Layer - an Experimental-Study. J Fluid Mech 197:453-477

Plesniak MW, Cusano DM (2005) Scalar mixing in a confined rectangular jet in crossflow. J Fluid Mech 524:1-45

Raman G, Rice EJ (1993) Core turbulence effect on naturally occuring modes in a circular jet. In: Ashpis D, Gatski TB, Hirsh R (eds) Instabilities and Turbulence in Engineering Flows. Fluid Mechanics and Its Applications, vol 16. Springer Netherlands, p 417

Rao SMV (2013) Experimental investigation on supersonic ejectors. Ph.D. thesis, Indian Institute of Science

Rao SMV, Asano S, Saito T (2016) Comparative studies on supersonic free jets from nozzles of complex geometry. Appl Therm Eng 99:599-612

Rao SMV, Jagadeesh G (2010) Vector Evaluated Particle Swarm Optimization (VEPSO) of Supersonic Ejector for Hydrogen Fuel Cells. J Fuel Cell Sci Technol 7

Rao SMV, Jagadeesh G (2014) Observations on the non-mixed length and unsteady shock motion in a two dimensional supersonic ejector. Phys Fluids 26

Rao SMV, Jagadeesh G (2015) Studies on the effects of varying secondary gas properties in a low entrainment ratio supersonic ejector. Appl Therm Eng 78:289-302

Sankaran S, Satyanarayana TNV, Annamalai K, Visvanathan K, Visvanathan B, Sundararajan T (2000) High altitude simulation of upper-stage rocket motors adopting second throat supersonic exhaust diffuser - A CFD approach. Proceedings of the 11th Conference on Astronautics: Opportunities and Challenges for Space Applications and Technology:383-392

Shelar VM, Hegde GM, Umesh G, Jagadeesh G, Reddy KPJ (2013) Visualization of coherent structures in turbulent subsonic jet using planar laser induced fluorescence of acetone. Eur Phys J-Appl Phys 62

Shelar VM, Hegde GM, Umesh G, Jagadeesh G, Reddy KPJ (2014a) Gas Phase Oxygen Quenching Studies of Ketone Tracers for Laser-Induced Fluorescence Applications in Nitrogen Bath Gas. Spectrosc Lett 47:12-18

Shelar VM, MV SR, Hegde G, Umesh G, Jagadeesh G, Reddy K (2014b) Acetone planar laser-induced fluorescence for supersonic flow visualization in air and nitrogen jet. International Journal of Mechanical and Materials Engineering 9:28

Shimshi E, Ben-Dor G, Levy A, Krothapalli A (2012) Experimental Investigation of Asymmetric and Unsteady Flow Separation in High Mach Number Planar Nozzles. In: Kontis K (ed) 28th International Symposium on Shock Waves. Springer Berlin Heidelberg, pp 129-134

Singhal G, Mainuddin, Tyagi RK, Dawar AL, Subbarao PMV (2010) Pressure recovery studies on a supersonic COIL with central ejector configuration. Opt Laser Technol 42:1145-1153

Slessor MD, Zhuang M, Dimotakis PE (2000) Turbulent shear-layer mixing: growth-rate compressibility scaling. J Fluid Mech 414:35-45

Spiegler E, Wolfshtein M, Manheimer-Timnat Y (1976) A model of unmixedness for turbulent reacting flows. Acta Astronaut 3:265-280

Stetsyuk V, Soulopoulos N, Hardalupas Y, Taylor AMKP (2016) Scalar dissipation rate statistics in turbulent swirling jets. Phys Fluids 28

Stratford BS, Beavers GS (1959) The calculation of the compressible turbulent boundary layer in an arbitrary pressure gradient a correlation of certain previous methods. Aeronautical Research Council Reports and Memoranda 3207

Su LK, Clemens NT (1999) Planar measurements of the full three-dimensional scalar dissipation rate in gas-phase turbulent flows. Exp Fluids 27:507-521

Sun MB, Geng H, Liang JH, Wang ZG (2009) Mixing Characteristics in a Supersonic Combustor with Gaseous Fuel Injection Upstream of a Cavity Flameholder. Flow Turbul Combust 82:271-286

Takahashi H, Hirota M, Oso H, Masuya G (2009) Measurement of Supersonic Injection Flowfield Using Acetone PLIF. T Jpn Soc Aeronaut S 51:252-258

Takahashi H, Ikegami S, Oso H, Masuya G, Hirota M (2008) Quantitative Imaging of Injectant Mole Fraction and Density in Supersonic Mixing. AIAA J 46:2935-2943

Tam CKW (1988) The Shock-Cell Structures and Screech Tone Frequencies of Rectangular and Non-Axisymmetric Supersonic Jets. J Sound Vib 121:135-147

Tam CKW, Tanna HK (1982) Shock Associated Noise of Supersonic Jets from Convergent-Divergent Nozzles. J Sound Vib 81:337-358

Thurber MC, Grisch F, Kirby BJ, Votsmeier M, Hanson RK (1998) Measurements and modeling of acetone laser-induced fluorescence with implications for temperature-imaging diagnostics. Appl Opt 37:4963-4978

Thurber MC, Hanson RK (1999) Pressure and composition dependences of acetone laser-induced fluorescence with excitation at 248, 266, and 308 nm. Appl Phys B-Lasers O 69:229-240

Thurber MC, Hanson RK (2001) Simultaneous imaging of temperature and mole fraction using acetone planar laser-induced fluorescence. Exp Fluids 30:93-101

Tropea C, Yarin A, Foss JF (2007) Springer Handbook of Experimental Fluid Mechanics. Springer Handbook of Experimental Fluid Mechanics. Springer-Verlag, Berlin Heidelberg

Vancruyningen I, Lozano A, Hanson RK (1990) Quantitative Imaging of Concentration by Planar Laser-Induced Fluorescence. Exp Fluids 10:41-49

Vishwakarma M, Vaidyanathan A (2016) Experimental study of mixing enhancement using pylon in supersonic flow. Acta Astronaut 118:21-32

Warhaft Z (2000) Passive scalars in turbulent flows. Annu Rev Fluid Mech 32:203-240

Zhu YH, Jiang PX (2014) Experimental and analytical studies on the shock wave length in convergent and convergent-divergent nozzle ejectors. Energy Convers Manage 88:907-914